

Two Dimensional Simulation of Laminar Flow Around a Couple of Bodies in Relative Motion

S. Noori *

Aerospace Research Institute,
Tehran, Iran
E-mail: s_noori@aut.ac.ir
*Corresponding author

F. Mahdavi

Aerospace Engineering,
Amirkabir University of Technology, Iran
E-mail: mahdavi@yahoo.com

S. M. H. Karimian

Aerospace Engineering,
Amirkabir University of Technology, Iran
E-mail: hkarim@aut.ac.ir

Received: 18 September 2011, Revised: 10 November 2011, Accepted: 8 April 2012

Abstract: In this paper an efficient dual time implicit approach is used to solve viscous laminar flow around a couple of bodies with general motion. The grid includes a background grid and two sets of grids around the moving bodies. Rotational and translational motions of the two bodies are managed separately in this grid arrangement. In this work the overset concept for hybrid grid is used and flow variables are interpolated implementing a simple method. The unsteady two dimensional Navier-Stokes equations are discretized using an implicit dual time stepping method. To accelerate convergence, the local pseudo-time stepping and implicit residual averaging are applied. To evaluate the present method, moving cases including rotational and translational motions are solved and the results are compared with experimental and numerical data.

Keywords: Compressible Flow, Laminar Flow, Moving Grid, Relative Motion

Reference: Noori, S., Mahdavi, F. and Karimian, S. M. H., 'Investigation of Oxygen Enriched Air Intake on Diesel Engine Exhaust Emissions', Int J of Advanced Design and Manufacturing Technology, Vol. 5/No. 3, 2012, pp. 29-37.

Biographical notes: **Noori, S.**, received her PhD in Aerospace Engineering from Amirkabir University of Technology 2006. She is currently Assistant Professor at the Aerospace Research Institute, Tehran, Iran. Her current research interest includes fluid mechanics and aerodynamic heating. **F. Mahdavi** was a student of aerospace engineering at the Amir kabir University of Technology. **S. M. H. Karimian** is Professor of Aerospace engineering at the Amirkabir University of Technology, Iran. He received his PhD in Mechanical engineering from Waterloo University of Canada. His current research focuses on fluid mechanics, thermodynamics and heat transfer.

1 INTRODUCTION

Simulations of unsteady compressible flows around moving bodies are extensively reported in aerospace literature. Analysis of oscillating airfoils, store separation, helicopter blades and other problems such as aeroelastic cases are some examples of moving body problems. Since the solution domain changes continuously in moving body problems, special care should be paid to retain the quality of grid. The simplest method for a moving boundary problem is to regenerate grid around the body after each step of its motion. Although this approach is desirable for structured grids [1], still it is a time consuming process. The other method is to restructure grids in regions close to the moving boundaries.

In this case, the moving boundary displacement at each time step must be less than the size of the smallest element in the region [2], [3]. The other method is based on the concept of dynamic mesh [4-6]. In this approach the computational grid deforms locally using a spring-analogy type algorithm. However, since this algorithm is iterative in nature with a high number of iterations, this approach is time consuming. For large motions overset grid can be used [7-9]. In this method each body has its own grid. On each grid, Chimera holes are defined in regions where the grid overlaps solid bodies belonging to the other grids.

Advantage of Chimera grid is its capability to simulate filed flow including several moving bodies around which high quality grids are generated. Disadvantage of this method, is that it requires a large number of interpolations. There are other methods which use hybrid grids in moving grid problems [10-13]. In this approach, the solution domain is divided into three zones to facilitate simulation of general body motion. The advantage of this method is that it is almost needless of node deletion/insertion process. Even in large translational displacements only a few elements are merged with each other.

This method was used by [12] to simulate the rotational/oscillational motion of a two-dimensional body. For the solution of unsteady Navier-Stokes equations they used upstream splitting method of AUSM [14]. Later Ali Sadeghi et al modified the method of [12] to provide a smoother grid movement in the solution domain. They solved unsteady viscous flow around a single body in motion. Extension of the work of [13] to inviscid flow simulation of two bodies in motion with respect to each other was carried out by Salehi et al [15]. In the present work, the method of [15] is generalized for the solution of viscous flow

around two bodies in relative motion with respect to each other. For this purpose boundary conditions of [13], [15] are modified as well.

Governing equation of viscous laminar flow is solved using implicit dual time stepping scheme of [6], [16]. An explicit Runge-Kutta multistage scheme is applied for iterating the solution in pseudo time in each time step. Convergence acceleration is increased with local pseudo-time stepping and implicit residual averaging [17]. Finally computational results are compared with experimental data. Also to demonstrate correct performance of the present method different benchmark problems, defined in this paper, are solved.

2 GRID GENERATION APPROACH

In the present study the grid generation method of Ref. 15 is used for the solution of Navier-Stokes equations around couple of bodies moving with respect to each other. As shown in Fig. 1a, cartesian grid is generated as the background grid in solution domain. In addition to the background grid, two other zones of grids are generated around body A. First zone contains a grid surrounding body A within a circular boundary. This grid is fixed to the body and moves with it. The second zone has a squared boundary and contains the grid surrounding the first zone. In translational motion of body A first and second zones will translate with the body but in rotational motion, it is only the first zone which will rotate with body A. In the rest of paper, the background grid and the aforementioned two surrounding grids are called grid A. Grid A provides general motion of body A.

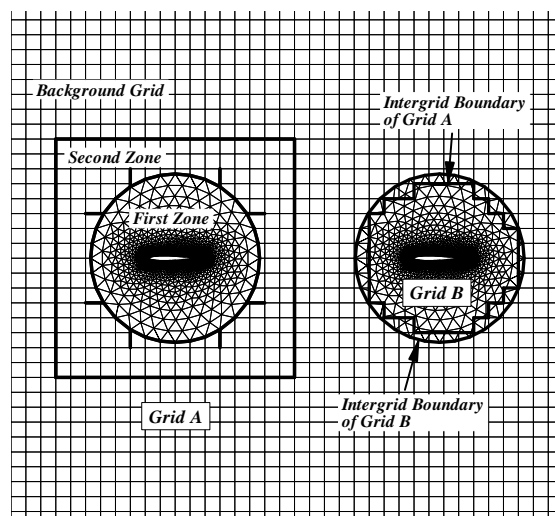


Fig. 1 Grid configuration surrounding bodies A and B

Body B will have rotational motion only. Therefore, any type of grid (structured, unstructured or hybrid grid) can be generated around it. As shown in Fig. 1a, in this study a triangular unstructured grid with a circular boundary is generated around body B; this grid is called grid B. Grid B is overset on the background grid. The solution strategy in the present study is to solve the whole flow field on two sets of grids A and B, separately. When the flow field is solved on grid A, the region within the intergrid boundary of grid A is excluded from the solution domain. Variables on the intergrid boundary of grid A are interpolated from the previous solution available on grid B. On the other hand, when the flow field is solved on grid B, the region within the intergrid boundary of grid B is excluded from the solution domain. Variables on the intergrid boundary of grid B are interpolated from the previous solution available on grid A. For more details about grid generation approach, refer to [15].

3 GOVERNING EQUATION

The two dimensional unsteady compressible viscous flow equations in the cartesian coordinate system can be written as

$$\frac{\partial}{\partial t} \int_{\Omega} w dx dy + \int_{\partial\Omega} (F^i - F^v) dy - (G^i - G^v) dx = 0 \quad (1)$$

where $w = (\rho, \rho u, \rho v, E)$ is the vector of conserved quantities, F^i and G^i represent the convective fluxes, and F^v and G^v describe the diffusion fluxes as given below

$$F^i = \begin{pmatrix} \rho u_r \\ \rho u_r u + P \\ \rho u_r v \\ (\rho E + p)u_r + u_m P \end{pmatrix}, \quad G^i = \begin{pmatrix} \rho v_r \\ \rho v_r u \\ \rho v_r v + P \\ (\rho E + p)v_r + v_m P \end{pmatrix}$$

$$F^v = \begin{pmatrix} 0 \\ \tau_{xx} \\ \tau_{xy} \\ u\tau_{xx} + v\tau_{xy} + q_x \end{pmatrix}, \quad G^v = \begin{pmatrix} 0 \\ \tau_{yx} \\ \tau_{yy} \\ u\tau_{xy} + v\tau_{yy} + q_y \end{pmatrix} \quad (2)$$

Variables ρ, P, u, v, u_r, v_r and E denote density, pressure, velocity components, relative velocities components and total energy, respectively. The relative velocities are defined as

$$u_r = u - u_m, \quad v_r = v - v_m \quad (3)$$

where u_m and v_m are the cartesian velocity components of control-volume boundary. Components of stress tensor are τ_{xx}, τ_{xy} and τ_{yx} , and q_x, q_y are components of heat flux vector. The viscosity coefficient μ , is calculated according to Sutherland's law. Equation (1) is augmented by the equation of state, which for a perfect gas is given by,

$$P = (\gamma - 1) \rho \left[E - \frac{u^2 + v^2}{2} \right] \quad (4)$$

Having discretized the solution domain to a number of control volumes with area of A_i , equation (1) then is written as

$$\frac{d}{dt} (w_i A_i) + R_i(w) - D_i(w) = 0 \quad (5)$$

where $R_i(w)$ is the sum of the convective and dissipative fluxes in x and y directions, and $D_i(w)$ is the numerical dissipative term [18] which is added to Eq. (1). This $D_i(w)$ is a combination of fourth and second order differences with coefficients that depend on the local pressure gradient. More details about this term can be found in [18].

4 IMPLICIT TIME INTEGRATION

A fully implicit time discretization (in real time) of Eq. (5) can be written as: [19]

$$\frac{d}{dt} (w_i^{n+1} A_i^{n+1}) + R_i(w^{n+1}) - D_i(w^{n+1}) = 0 \quad (6)$$

Using second order accurate Backward Difference Formula [20] to discretize the transient term of the above equation will result in

$$\frac{3}{2\Delta t} (w_i^{n+1} A_i^{n+1}) - \frac{2}{\Delta t} (w_i^n A_i^n) + \frac{1}{2\Delta t} (w_i^{n-1} A_i^{n-1}) + R_i(w^{n+1}) - D_i(w^{n+1}) = 0 \quad (7)$$

A Dual Time Stepping method is used to solve this coupled nonlinear equation [20]. This is carried out through solving the following equation in each time step.

$$\frac{\partial w}{\partial \tau} + R^*(w^n) = 0 \quad (8)$$

where τ is pseudo-time, and $R^*(w^n)$ is the unsteady residual defined as

$$R^*(w^n) = \frac{3}{2\Delta t}(w_i^{n+1}A_i^{n+1}) - \frac{2}{\Delta t}(w_i^n A_i^n) + \frac{1}{2\Delta t}(w_i^{n-1}A_i^{n-1}) + R_i(w^{n+1}) - D_i(w^{n+1}) \quad (9)$$

Equation (8) defines a modified steady state problem in pseudo-time and is solved using explicit Runge-Kutta multistage method [20].

5 OVERSET IMPLEMENTATION

As mentioned earlier, governing equations are solved on two sets of grids iteratively. At each time step, the system of equations are solved on grid A which has outer flow boundary and its own intergrid boundary, as shown in Fig.1. For this purpose boundary conditions on intergrid boundary A are interpolated from the most updated values flow variables on grid B. From these results on grid A, flow variables along the intergrid boundary B are interpolated to provide boundary conditions for the solution of flow field on grid B. After the solution of flow field on grid B, the same process can be repeated until the error between intergrid boundary values of two successive iterations for both grids A and B becomes less than a desired value.

6 BOUNDARY CONDITIONS

At the far field, non-reflecting boundary conditions are implemented based on the characteristic analysis. At the solid wall boundary, zero mass flux is employed, and fluid velocity is set equal to the speed of airfoil surface at that point. If the airfoil is stationary, the fluid velocity would be zero.

7 SOME DETAILS ABOUT VISCOUS TERM CALCULATIONS

For the calculation of viscous fluxes, first derivatives of velocity components should be evaluated on the control volume surfaces. The method of [13] is used for this purpose. As shown in Fig. 2a, using Green theorem first derivative of velocity component on edge AB is approximated by the line integral velocity component along the edges of AP-PB-BK-KA, divided by the area of APBK. On the inter-grid boundaries, shown in Fig. 2b, the area on which integral is carried out would be APB. For instance $\frac{\partial u}{\partial x}$ on the AB edge of Fig. 2b will be calculated as follows,

$$\frac{\partial u}{\partial x} \approx \frac{1}{\Omega_{APB}} \oint_{APB} u dy = \frac{(u_A + u_B)\Delta y_{AB} + (u_B + u_P)\Delta y_{BP} + (u_P + u_A)\Delta y_{PA}}{2A_{APB}} \quad (10)$$

Other derivatives of velocity components will be calculated in the similar manner.

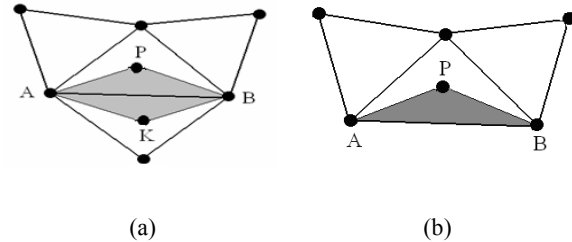


Fig. 2 Area to be integrated for the calculation of velocity derivatives on AB edge a) Edge within the boundary, b) Edge along the intergrid boundaries

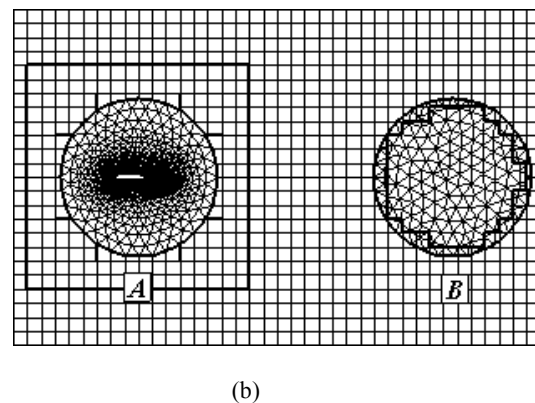
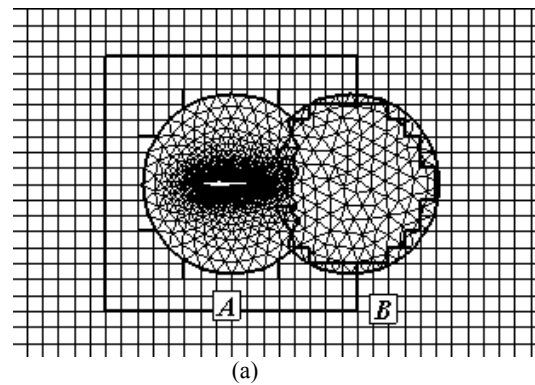


Fig. 3 a) Clean grid close to body A, and b) Clean grid far from body A

8 RESULTS AND DISCUSSION

In this section the method is validated through the simulation of laminar flow over moving bodies. Results

are compared with the experimental data and other numerical results.

In order to verify the solution algorithm on two sets of grids as described before, steady state flow of Mach=0.8 and Re=73 over a NACA0012 airfoil at 10 degrees angle of attack is considered on two different grid configurations. The airfoil is set in grid A, and grid B is clean. Grid configurations shown in Fig. 3 are, a) clean grid close to body A, and b) clean grid far from body A. In Fig. 3a grid B is close to grid A, forming an overlapping region. In Fig. 3b, however grid B is far from grid A and no overlapping region is formed.

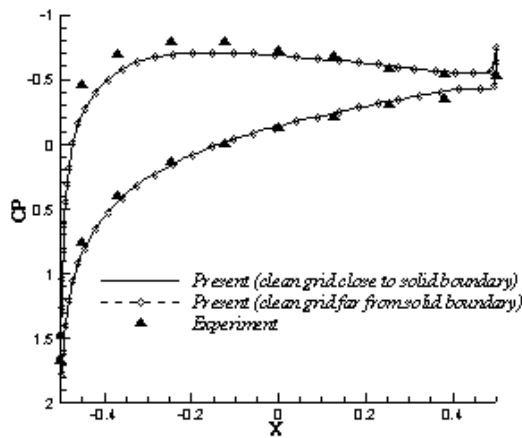


Fig. 4 Comparison of surface pressure coefficient distributions: present results and experimental data; NACA 0012 airfoil at M= 0.8, Re=73, $\alpha=10^\circ$

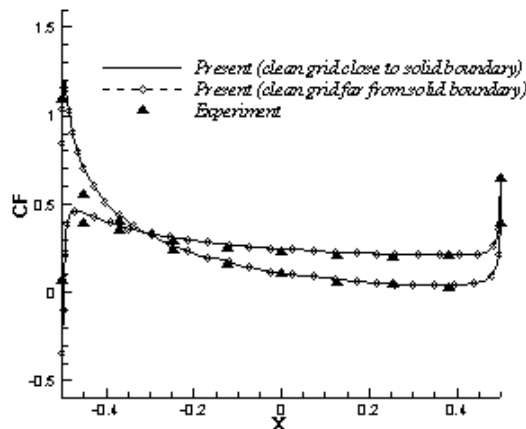


Fig. 5 Comparison of surface force coefficient distribution: present results and experimental data; NACA 0012 airfoil at M= 0.8, Re=73, $\alpha=10^\circ$

Figs. 4 and 5 illustrate the comparison of pressure coefficient distribution and surface force coefficient distribution on the surface of airfoil with the experimental data [21]. Excellent agreement of results obtained on both grids with each other shows that the solution is independent of location of grids A and B.

They are also in excellent agreement with the experimental data except at the leading edge where a little difference is seen.

Again to demonstrate the independence of solution strategy from the grid arrangement and also the accuracy of interpolation stencil used in the overlapping layer, flow field of the 1st test case is solved on two different grids shown in Fig.6. These include, a) body is set in grid A and grid B is clean, and b) body is set in grid B and grid A is clean.

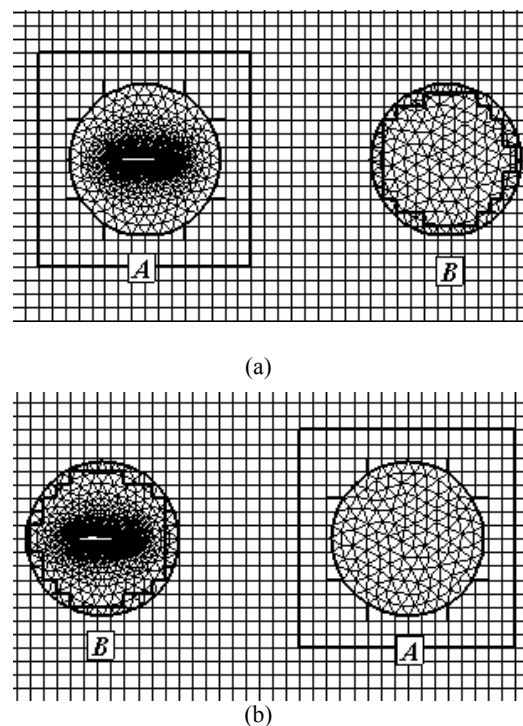


Fig. 6 a) Body A and clean grid B, and b) Body B and clean grid A.

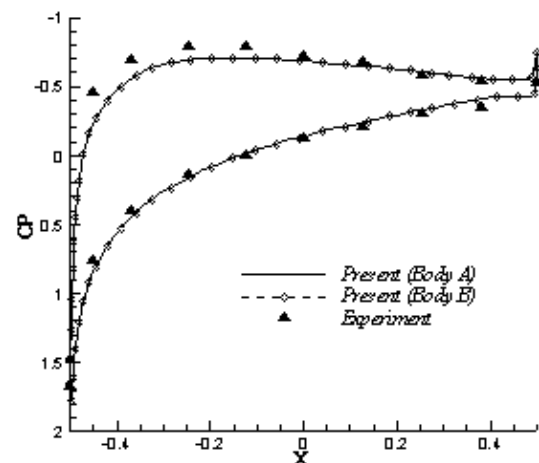


Fig. 7 Comparison of surface pressure coefficient distribution; present results and experimental data; airfoil NACA 0012 at M= 0.8, Re=73, $\alpha=10^\circ$

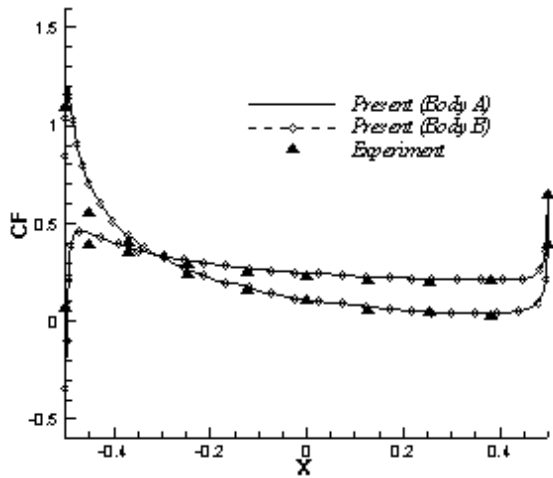


Fig. 8 Comparison of surface force coefficient distribution; present results and experimental data; airfoil NACA 0012 at M= 0.8, Re=73, $\alpha=10^\circ$.

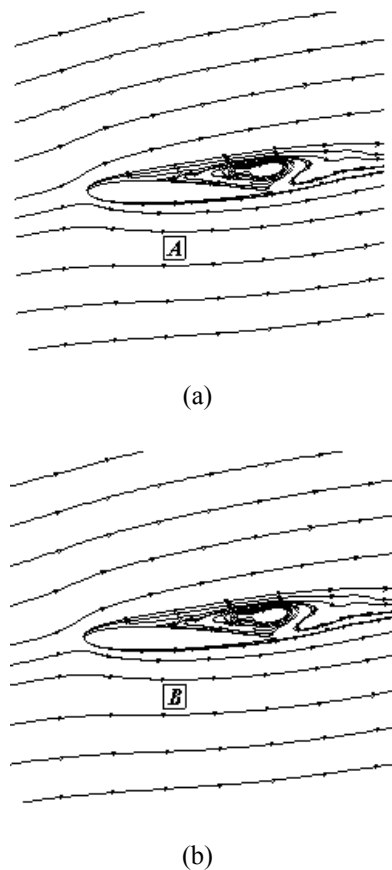


Fig. 9 stream lines in flow separation zone for grid configurations of Fig. 5. NACA 0012 airfoil at M= 0.8, Re=500, $\alpha=10^\circ$, a) Body A and clean grid B, and b) Body B and clean grid A

Fig. 7 depicts comparison of surface pressure coefficient distributed over two grids and also compared with experimental data [21]. Same comparison is made for surface force coefficient distribution in Fig. 8. Again results obtained on two grids are in excellent agreement with each other. In the third case, steady state flow at Mach 0.8, Re=500 and $\alpha=10^\circ$ are solved on the grids of Fig. 6. This flow includes a separation zone. This separation has been captured by the present solution, as shown in Fig. 9.

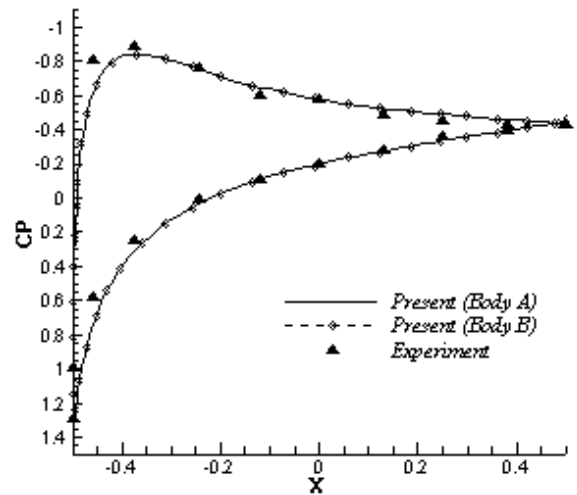


Fig. 10 Comparison of surface pressure coefficient distribution; present results and experimental data; airfoil NACA 0012 at M= 0.8, Re=500, $\alpha=10^\circ$

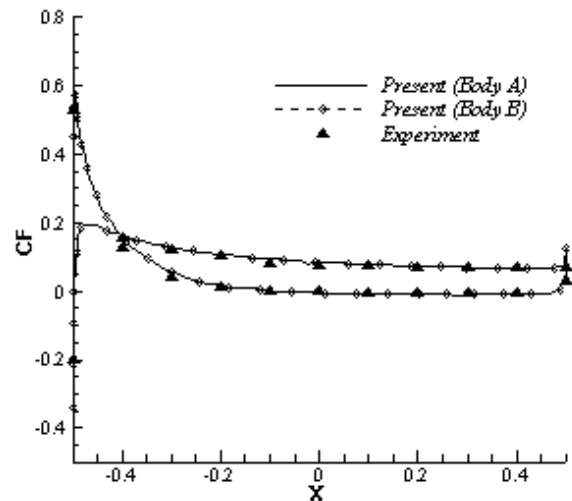


Fig. 11 Comparison of surface force coefficient distribution; present results and experimental data; airfoil NACA 0012 at M= 0.8, Re=500, $\alpha=10^\circ$

As seen, results are exactly similar to each other revealing grid configuration independency of the

algorithm. Comparison of pressure coefficient distribution obtained over these two grids and also compared with experimental data [21] is shown in Fig. 10. Same comparison is shown for surface force coefficient distribution in Fig. 11.

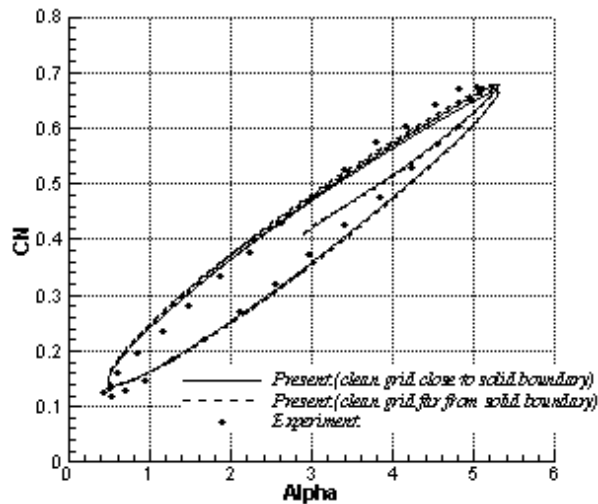


Fig. 12 Comparison of normal-force coefficient loop; present results and experimental data, AGARD CT1 test case; airfoil NACA 0012

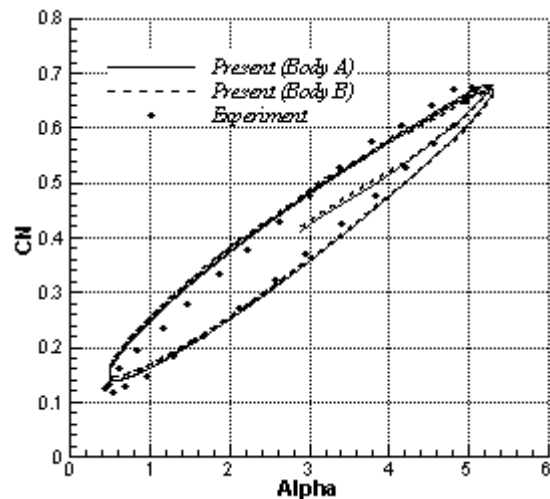


Fig. 13 Comparison of normal-force coefficient loop; present results and experimental data, AGARD CT1 test case; airfoil NACA 0012

Results of the present study agree very well with each other and also with experimental data. A supersonic case of Mach=2 and Re=1000 over a NACA 0012 airfoil at $\alpha=10^\circ$ was also solved on grids of Fig. 6. Results are not reported here. Again, they were in excellent agreement with each other. All of the steady

state solutions are obtained after 5000 local time steps in real time.

As the fourth test case, we would like to solve the unsteady flow over the oscillatory pitching airfoil of NACA 0012, defined in AGARD CT1 test case [22]. This test case has been widely studied in the literature. Grids of Fig 2 are used for the simulation of CT1 unsteady flow. Consider the harmonic pitching motion of airfoil about the quarter chord of it with the following time dependent varying angle of attack,

$$\alpha = \alpha_m + \alpha_0 \sin \omega t$$

where α_m is the mean angle of attack, α_0 is the amplitude of its oscillation, and ω is the angular frequency of the motion, related to reduced frequency, k , by

$$k = \frac{\omega c}{2U_\infty}$$

In this relation, U_∞ is the free stream velocity and c is the chord length of the airfoil. Flow conditions are

$$M_\infty = 0.6, \alpha_m = 2.89, \alpha_0 = 2.41, k = 0.0808, Re = 4.8 \times 10^6$$

Unsteady solution is obtained using local pseudo time steps, and real time step of 5.2E-3 s. The above problem is solved on two different grids shown in Fig.3. As shown in Fig. 3a, the oscillating airfoil would be within grid A. Grid B is close to grid A, forming an overlapping region. In Fig. 3b, however the oscillating airfoil is set within grid A. Grid B is far from grid A and no overlapping region exists. Numerical calculation of unsteady flow starts from the steady state solution of Mach 0.6 with Re=4,800,000 over NACA 0012 airfoil at 2.41 degrees angle of attack. The variations of normal force coefficient obtained from the present method on both grids are compared with experimental data in Fig. 12.

Results obtained on both grids are in excellent agreement with each other. Moreover, results of the present study agree very well with the results of the experiment [22]. The difference between numerical results and experimental data observed here has been reported by other researchers in the literature, as well [11], [23]. This difference can be eliminated if α_m is changed slightly.

Once again to demonstrate grid configuration independency of the algorithm in a moving body problem, the CT1 test case is solved on grids of Fig. 6. The variations of normal force coefficient obtained from the present method on both grids are compared with the experimental data in Fig. 13. Results obtained on both grids are in excellent agreement with each other, and with the experimental data. For translational-rotational motion, the fifth test case is defined. Two cases with the same physics of flow field are considered, in Fig. 14. Two NACA0012 airfoils are

located at a distance equal to 140 chords from each other. In the first case, the left airfoil is stationary and the oscillating airfoil at the right moves toward the left with Mach 0.5 in a stationary air.

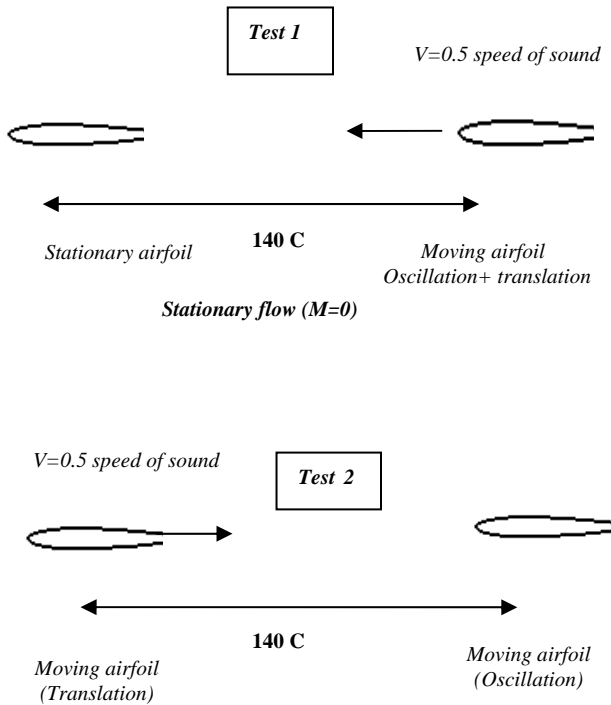


Fig. 14 Illustration of test definition for rotational-translational motion of two bodies with respect to each other

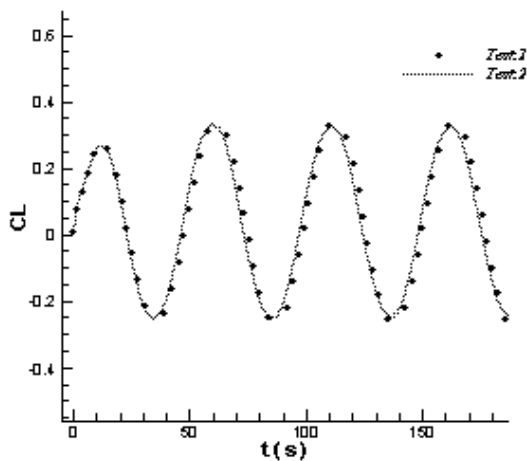


Fig. 15 Lift coefficient history of NACA0012 airfoil for rotational-translational motion, tests 1 and 2 of 7th case

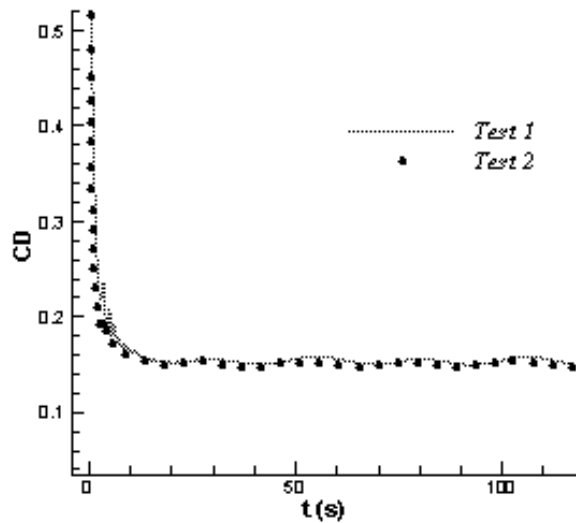


Fig. 16 Drag coefficient history of NACA0012 airfoil for rotational-translational motion, tests 1 and 2 of 7th case.

9 CONCLUSION

In the second case, the airfoil at the left and the air move together with Mach 0.5 and $Re=10,000$ toward the stationary oscillating airfoil at the right. Parameters governing the oscillating airfoil are $\alpha_m = 0$, $\alpha_0 = 2.51$, $k = 0.0814$. Unsteady solution is obtained using local pseudo time steps and real time step of $2.55E-2$ s. Lift and drag coefficient histories of the right airfoil in both cases are compared with each other in Figs. 15 and 16. The excellent agreement shows the accuracy of the algorithm for simulation of unsteady problems. The little difference between the two results is due to the differences between the grids generated around the right airfoil in two cases.

The moving mesh algorithm of [15] is extended to solve two-dimensional compressible laminar flow around two bodies in relative motion with respect to each other. Definition of two grid zones has provided the capability of simulating translational and rotational motion of bodies easily. This algorithm is validated on different grid configurations to prove accuracy of interpolation stencil used in this study. The correct performance of algorithm strategy on two sets of grids A and B sequentially has been demonstrated on various grid configurations. Compressible flow is solved on two moving body benchmark problems, and defined in this study, to show capability of the present algorithm in capturing accurate results.

REFERENCES

- [1] Gationde, A. L., "A dual-time for solution of the unsteady navier-stokes equation", *Aeronautical J.*, Vol. 98, pp. 283-291, 1994.
- [2] Goswami A. and Parpia I. H., "Grid restructuring for moving boundaries", *AIAA Paper*, No. 91-1589-CP, 1991.
- [3] Trepanier J. Y., Reggio M., and Camarero R., "Unsteady navier-stokes solution for arbitrary moving bodies and boundaries", *AIAA paper*, No. 92-0051, 1992.
- [4] Batina, J. T., "Unsteady navier-stokes algorithm with unstructured dynamic mesh for complex-aircraft aerodynamic analysis", *AIAA Journal*, Vol. 29, No. 3, 1991, pp. 327-33.
- [5] Tsai, H. M. and Wong, A. S. F. et al., "Unsteady flow calculations with a parallel multiblock moving mesh algorithm", *AIAA Journal*, Vol. 39, No. 6, June 2001, pp.1021-1029.
- [6] Jahangirian A., and Hadidolabi M., "An implicit solution of the unsteady navier-stokes equations on unstructured moving grids", 24th International Congress of the Aeronautical Science, 2004.
- [7] Steger J. L., Dougherty F. C., and Benek J. A., "A chimera grid scheme, advances in grid generation", edited by K. N. Ghia and U. Ghia, FED-Vol. 5, American Society of Mechanical Engineers, New York, 1983.
- [8] Benek J. A., Buning, P. G., and Steger, J. L., "A 3-D chimera grid embedding technique", *AIAA Paper* 85-1523, June 1985.
- [9] Nakahashi K., Togashi, F., and Sharov, D., "Intergrid-boundary definition method for overset unstructured grid approach", *AIAA Journal*, Vol. 38, No. 11, November 2000, pp. 2077-2084.
- [10] Aftosmis M. J., Berger M. J., and Melton J. E., "Robust and efficient cartesian mesh generation for component-based geometry", *AIAA Paper* No. 97-0196, 1997.
- [11] Mirsajedi S. M., Karimian S. M. H., and Mani M., "A multizone moving mesh algorithm for simulation of flow around a rigid body with arbitrary motion", *ASME Journal of Fluids Engineering*, Vol. 128, 2006, pp. 297-304.
- [12] Mirsajedi S. M. and Karimian S. M. H., "Evaluation of a two-dimensional moving-mesh method for rigid body motions", *Aeronautical Journal*, Vol. 110, 2006, pp. 429-438.
- [13] Alisadeghi, H., Karimian, S. M. H. and Jahangirian, A. R., "An implicit dual time stepping algorithm for hybrid dynamic meshes", 14th Annual Conference of The Computational Fluid Dynamics, Canada, July 2006.
- [14] Liou M, and Steffen C. J., "A new flux splitting scheme", *Journal of Computational physics*, Vol. 107, 1993, pp. 23-39.
- [15] Salehi, F. S, and Karimian, S. M. H, "Moving mesh method for relative motion of two bodies", The 7th conference of Iranian Aerospace Society, Sharif University of Technology, February 19-21, 2008.
- [16] Jameson A., "Time-dependent calculations using multi-grid, with applications to unsteady flows past airfoils and wings," *AIAA Paper* No 91-1596, 1991.
- [17] Jameson A., Schmidt W. and Turkel E., "Numerical solution of the navier-stokes equations with finite volume methods using runge-kutta time stepping schemes", *AIAA Paper* 81-1259, 1981.
- [18] Jameson A. and Mavriplis D., "Finite volume solution of the two dimensional navier-stokes equation on a regular triangular mesh", *AIAA Journal*, Vol. 24, No. 4, 1986.
- [19] Jameson A., "Time-dependent calculations using multi-grid, with applications to unsteady flows past airfoils and wings", *AIAA Paper* No. 91-1596, 1991.
- [20] Jahangirian A., and Hadidoolabi M., "An implicit solution of the unsteady navier-stokes equations on unstructured moving grids", 24th International Congress of the Aeronautical Science, Yokohama, Japan, 2004.
- [21] Bristeau, M. Glowinski, R., Periaux, J. and Vivand, H., "Numerical simulation of compressible navier-stokes flow", Federal Republic of Germany, Friedr. Vieweg und Sohn, 1987, pp. 349.
- [22] Advisory Group for Aerospace Research and Development NEUILLY-SUR-SEINE "Compendium of Unsteady Aerodynamic Measurements", Report No. AGARD-702, 1982.
- [23] Jahangirian, A., and Hadidoolabi, M., "Unstructured moving grids for implicit calculation of unsteady compressible viscous flow", *International Journal for Numerical Methods in Fluids*, Vol. 47, 2005, pp. 1107-1113.